Imaging of Dynamic Secretory Vesicles in Living Pollen Tubes of *Picea meyeri* Using Evanescent Wave Microscopy[1][W]

Xiaohua Wang, Yan Teng, Qinli Wang, Xiaojuan Li, Xianyong Sheng, Maozhong Zheng, Jozef Šamaj, František Baluška, and Jinxing Lin*

Key Laboratory of Photosynthesis and Molecular Environment Physiology, Institute of Botany, Chinese Academy of Sciences, Beijing 100093, China (X.W., Q.W., X.L., X.S., M.Z., J.L.); Graduate School of the Chinese Academy of Sciences, Beijing 100049, China (X.W., Q.W., X.L., M.Z.); Institute of Biophysics, Chinese Academy of Sciences, Beijing 100101, China (Y.T.); Institute of Cellular and Molecular Botany, Department of Plant Cell Biology, Rheinische Friedrich-Wilhelms-University Bonn, D–53115 Bonn, Germany (J.Š., F.B.); Institute of Botany, Slovak Academy of Sciences, SK–84223, Bratislava, Slovak Republic (J.Š.); and Institute of Plant Genetics and Biotechnology, Slovak Academy of Sciences, SK–95007, Nitra, Slovak Republic (F.B.)

Evanescent wave excitation was used to visualize individual, FM4-64-labeled secretory vesicles in an optical slice proximal to the plasma membrane of *Picea meyeri* pollen tubes. A standard upright microscope was modified to accommodate the optics used to direct a laser beam at a variable angle. Under evanescent wave microscopy or total internal reflection fluorescence microscopy, fluorophores localized near the surface were excited with evanescent waves, which decay exponentially with distance from the interface. Evanescent waves with penetration depths of 60 to 400 nm were generated by varying the angle of incidence of the laser beam. Kinetic analysis of vesicle trafficking was made through an approximately 300-nm optical section beneath the plasma membrane using time-lapse evanescent wave imaging of individual fluorescently labeled vesicles. Two-dimensional trajectories of individual vesicles were obtained from the resulting time-resolved image stacks and were used to characterize the vesicles in terms of their average fluorescence and mobility, expressed here as the two-dimensional diffusion coefficient D^2. The velocity and direction of vesicle motions, frame-to-frame displacement, and vesicle trajectories were also calculated. Analysis of individual vesicles revealed for the first time, to our knowledge, that two types of motion are present, and that vesicles in living pollen tubes exhibit complicated behaviors and oscillations that differ from the simple Brownian motion reported in previous investigations. Furthermore, disruption of the actin cytoskeleton had a much more pronounced effect on vesicle mobility than did disruption of the microtubules, suggesting that actin cytoskeleton plays a primary role in vesicle mobility.

Vesicle trafficking is fundamental to numerous activities in eukaryotic organisms and underlies many of the basic processes involved in cell growth and differentiation. The vesicle trafficking network is responsible for exocytosis and endocytosis (Rothman, 1994; Bretscher and Aguado-Velasco, 1998; Hepler et al., 2001; Zefirov et al., 2004; Šamaj et al., 2005). Exocytosis is the process by which secretory vesicles derived from the trans-Golgi network (TGN) attach and/or fuse with the plasma membrane, releasing their contents into the extracellular space. In contrast, endocytosis is responsible for the uptake of compounds from the extracellular milieu to be used in cellular metabolism, the uptake of signal molecules, and the uptake of membrane proteins and lipids to be recycled (Šamaj et al., 2005). Vesicle transport of cargo is carried out by coated vesicles from a donor compartment. These vesicles move on to the Golgi apparatus, where further posttranslational modifications are made. Uncoating and subsequent docking and fusion of the vesicles with a target compartment membrane then occur. Three major types of vesicle coating proteins, COPI, COPII, and clathrin, are involved in exocytotic and endocytotic vesicle trafficking. Plant cells grow when secretory vesicles derived from the TGN and endosomes fuse with the plasma membrane, into which they insert cellulose synthases. At the same time, they deliver cell wall matrix into the cell wall (Kimura et al., 1999; Emons and Mulder, 2000).

The last few decades have witnessed many studies of vesicle trafficking, but most studies have focused on

[1] This work was supported by the National Science Fund of China for Distinguished Young Scholars (grant no. 30225005) and a grant for general program (no. 30570100), together with grants from Deutsche Forschungsgemeinschaft (no. SA 1564/2–1 to J.Š.); from EU Research Training Network TIPNET (project no. HPRN–CT–2002–00265) obtained from Brussels, Belgium; from Slovak grant agency APVV (no. APVT–51–002302; Bratislava, Slovakia); from Slovak grant agency VEGA (no. 2/5085/25; Bratislava, Slovakia); and from Deutsches Zentrum für Luft- und Raumfahrt (Bonn).

* Corresponding author; e-mail linjx@ibcas.ac.cn; fax 0086–10–62590833.

The author responsible for distribution of materials integral to the findings presented in this article in accordance with the policy described in the Instructions for Authors (www.plantphysiol.org) is: Jinxing Lin (linjx@ibcas.ac.cn).

[W] The online version of this article contains Web-only data.

Article, publication date, and citation information can be found at www.plantphysiol.org/cgi/doi/10.1104/pp.106.080168.

animal cells (Rutter and Tsuboi, 2004; Sudhof, 2004; Vo et al., 2004; Zanner et al., 2004; Wang and Quick, 2005; Xu et al., 2005). Relatively few studies of vesicle trafficking in plant cell systems have been performed, largely due to the difficulties presented by the plant cell walls. However, in a study on vesicle transport during pollen tube growth, Derksen et al. (1995) used transmission electron microscopy (TEM) to quantitatively analyze the distribution and density of vesicles in cryo-fixed tobacco (*Nicotiana tabacum*) pollen tubes. Using video microscopy and TEM, Ketelaar (2002) subsequently estimated the number of exo- and endocytotic vesicles in Arabidopsis (*Arabidopsis thaliana*) root hairs and proposed that the exocytosis and endocytosis rates were 4,202 and 6,901 vesicles per minute, respectively. Although indirect insight can be gained from electron microscopy or optical recording with confocal microscopy (Picton and Steer, 1983; Rutten and Knuiman, 1993; Parton et al., 2001, 2003), neither method can easily provide the high temporal resolution and information needed to determine the frequency or rate of fast exocytotic and endocytotic events occurring during pollen tube growth. By means of differential interference contrast microscopy, Foissner et al. (1996) recorded vesicle trafficking in the characean wound wall system. de Win et al. (1998) applied interactive computer-assisted video microscopy to analyze the movement patterns of the organelles in pollen tubes and found the movements were random in the tip regions. Sieberer and Emons (2000) measured the speed and orientation of organellar motion in root hairs of *Medicago truncatula* with diameters of 1 to 2 μm using video microscopy. Indeed, to our knowledge, no study to date has portrayed the dynamic motion of individual secretory vesicles in living pollen tubes (for studies of tip-growing root hairs, see Ovecka et al., 2005).

With the introduction of evanescent wave microscopy (EWM), direct monitoring of an individual vesicle during secretion has become possible (Tsuboi and Rutter, 2003; Kuhn and Pollard, 2005). Evanescent wave excitation of fluorescence is based on the decaying near-field generated near a dielectric interface upon the total internal reflection of light. Due to the light confinement of evanescent wave excitation, photobleaching and phototoxic reactions are generally of minor concern, as compared to conventional epi-excitation or confocal laser scanning microscopy. Therefore, EWM provides an ideal tool for long-term observations or when time-resolved imaging at high frame rates is desired.

In this study, we visualized secretory vesicle motions in living pollen tubes after labeling the vesicles with the endocytotic/exocytotic tracer FM4-64. This amphiphilic styryl dye has been used to investigate endocytosis and visualize the diverse membrane compartments in living fungal hyphae (Fischer-Parton et al., 2000). FM4-64 is a suitable probe for imaging the dynamic changes in size, morphology, and position of apical vesicles within growing pollen tubes because of its staining pattern, relatively high photostability, and low cytotoxicity (Bolte et al., 2004). Thus, it is an excellent dye for following dynamic processes in living cells over time without disturbing these processes (Šamaj et al., 2005; Dettmer et al., 2006; Šamaj, 2006). In this study, we used EWM for two-dimensional (2-D) secretory vesicle tracking to determine the role of the actin cytoskeleton and microtubules in vesicle trafficking and dynamics proximal to the plasma membrane.

RESULTS

Visualization of Secretory Vesicles Close to the Plasma Membrane in Living Pollen Tubes

Pollen tubes labeled with FM4-64 exhibited a distinct peripheral, bright staining pattern (Fig. 1A). Confocal microscopic analysis of labeled pollen tubes demonstrated that the peripheral staining was plasma membrane associated, not cell wall associated, as indicated by plasmolysis with 100 μM sorbitol in the presence of FM4-64 (Fig. 1C). Pretreatment of pollen tubes with 500 μM sodium azide impaired dye uptake; therefore, FM4-64 fluorescence could be observed only at the plasma membrane (Fig. 1E), but still allowed staining of the plasma membrane of the apical and subapical regions. Because FM4-64 is a membrane-selective fluorescent dye and does not label the cytoplasm or cell wall (Fig. 1C), it was used to detect vesicle trafficking in living pollen tubes.

Under EWM, apical region versus subapical region defined by de Win et al. (1996) and Wang et al. (2005) can be mostly distinguished because the apical region in *Picea meyeri* tubes with FM4-64 staining appeared crescent, which was different from inverted cone-shaped (V-shaped) clear zone in angiosperm pollen tubes. Fluorescent spots were distributed plentifully over the apical and subapical regions beneath the plasma membrane of the pollen tube proximal to the coverslip. The spot morphologies of the apical and subapical spots were similar. The density of spots, however, was much higher in the apical region than in the subapical region (Fig. 1G). The spots appeared dim because of the scattering effect induced by out-of-focus vesicles or organelles, such as the Golgi apparatus and endoplasmic reticulum deeper within the pollen tube cytoplasm (Fig. 1H). After processing with flattening and high-pass filters, the spots became clear and could be seen to have similar sizes (Fig. 1I). Spots were identified as vesicles when the average intensity in a 3- $\times$ 3-pixel region was 20% greater than the surrounding background gray value in three consecutive frames, the central intensity was a local maximum, and the spot was present in more than three consecutive images. Because the diameter of vesicles in *P. meyeri* ranged from 100 to 300 nm (Wang et al., 2005), twice the size as those in Lilium and Arabidopsis under the TEM, only those spots

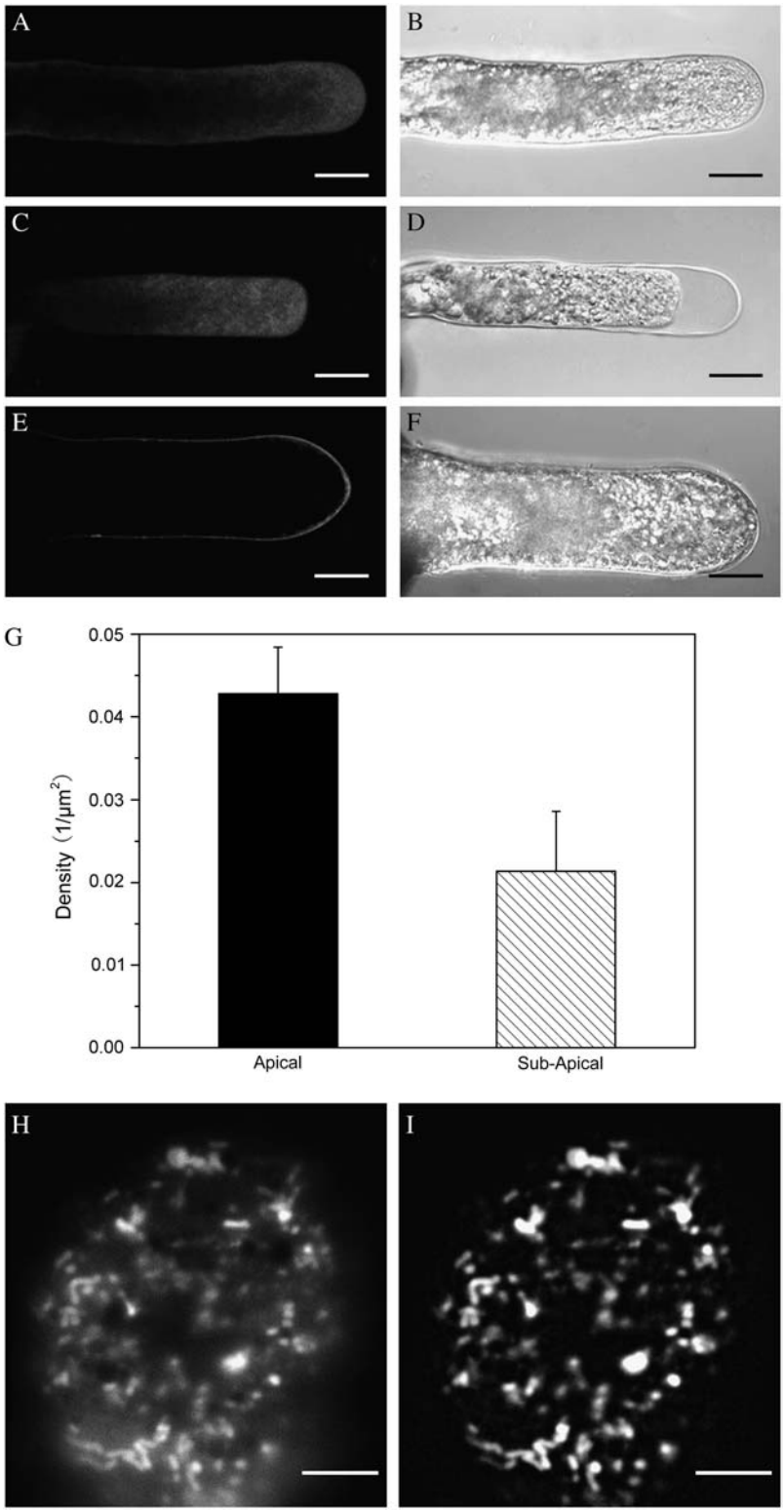

Figure 1. Secretory vesicles in living pollen tubes of *P. meyeri*. A, A median focal plane optical section showing a typical FM4-64 staining pattern in a growing pollen tube. B, Corresponding bright-field image to A. C, Applying standard medium with 100 μM sorbitol and 2 μM FM4-64 showed dye fluorescence associated with retracted protoplast but not with cell wall. D, Corresponding bright-field image to C. E, Sodium azide impaired FM4-64 uptake. Note that dye remains at the plasma membrane. F, Corresponding bright-field image to E. G, Density of the vesicles in apical and subapical regions in pollen tubes ($n = 8$). H, First image in a stack of 500 taken at 200-ms intervals observed under evanescent wave microscope. I, Flattened and low-pass filtered image of H. For filtering, blurred versions of images on the left were first generated by flatten filtering and then enhanced with low-pass filter three times, at last yielding the distinct images by executing contrast enhancement. Bar = 25 μm for A to F, 5 μm for H and I.

with diameter less than 400 nm were considered as secretory vesicles (TGN vesicles) for analysis; other larger fluorescent spots are considered not to be vesicles or organelles, which were excluded from analysis in this article.

Dynamics of FM4-64-Labeled Secretory Vesicles in Living Pollen Tubes

To explore vesicle motions, a series of images of growing pollen tubes labeled with FM4-64 was taken under EWM. Movies compiled from a large number

of images showed that the vesicles moved around a resting position in the apical and subapical regions of the pollen tubes (Supplemental Movies 1 and 2). These bright fluorescent spots showed short, nonlinear motions in various directions in living pollen tubes. Furthermore, two types of secretory vesicle mobility were observed along the pollen tubes in terms of running length and velocity: short-distance motion (Fig. 2A) and long-distance motion (Fig. 2B). Long-distance motions were defined as motions of >1 μm in distance and with a maximum velocity of >2 μm/s. All other motions were considered short-distance motions. Approximately 10% of vesicles within the evanescent field could be classified as undergoing long-distance motion, whereas the majority (>80%) of vesicles proximal to the plasma membrane underwent short-distance motion.

Short-distance motions often involved rapid changes or reversals in direction and velocity between consecutive runs, whereas the long-distance motions were directed to the apical region, as though these vesicles were guided to their targets. Moreover, the two types of motion differed in their velocities. The average velocity during short-distance motions was 1.09 ± 0.02 μm/s ($n = 30$ vesicles), with a maximum velocity of 3.5 μm/s. The run length averaged 75 ± 0.8 μm ($n = 30$ vesicles), with a duration of 100 s. In contrast, the average velocity during long-distance motions was 1.93 ± 0.05 μm/s ($n = 30$ vesicles), and the maximum velocity was 5.85 μm/s (Table I). In addition, vesicle motion could be estimated by the mean squared displacement (MSD) and the diffusion coefficient. The diffusion coefficient in two dimensions, D^2, was derived from the slope of a plot of the MSD versus time for $\Delta t \rightarrow 0$ (Fig. 2, C and D). For

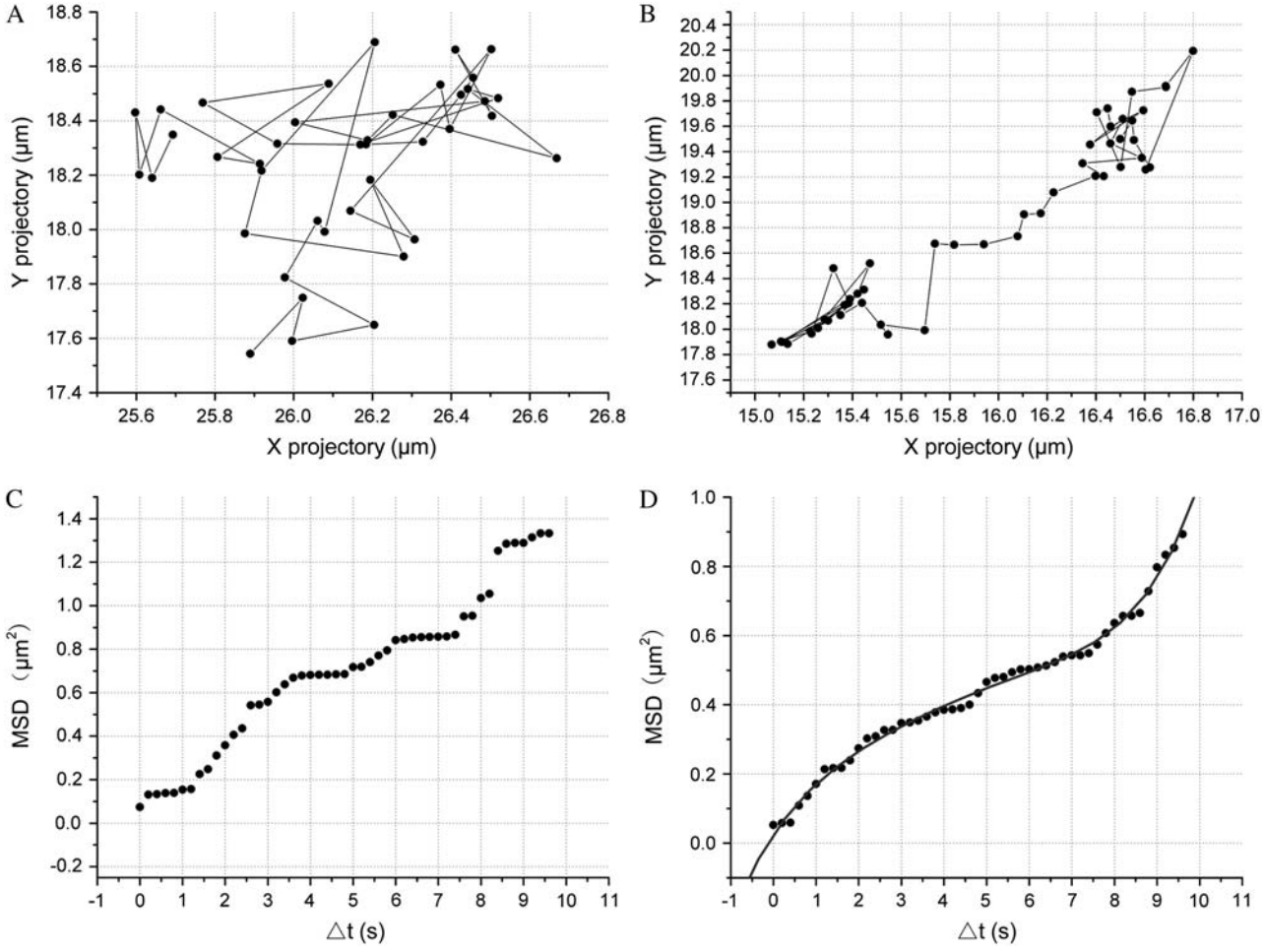

Figure 2. Short-distance and long-distance motions of secretory vesicles in *P. meyeri* pollen tubes. A, The lateral mobility of a short-distance motion vesicle on a plot of *x* versus *y* coordinates. B, The lateral mobility of a long-distance motion vesicle on the plots of *x* versus *y* coordinates. C, MSD of short-distance motion plotted against time interval Δt. To calculate the MSD, we measured the distance of motion over an interval of fixed duration (0.2 s), with the interval starting first at 0 ms after the beginning of the recording, then at 200 ms, at 400 ms, and so on until at 9.6 s. All distances were squared. D, MSD of long-distance motion plotted against time interval Δt. The characteristic decay time of the MSD is given by a polynomial fit (black line).

Table I. *Two types of secretory vesicle mobility based on measurements of 30 vesicles observed under EWM in living pollen tubes*

The vesicles we observed under EWM were considered as secretory TGN vesicles. Only those spots with diameter less than 400 nm were considered as vesicles for analysis, and other larger fluorescent spots bigger than 400 nm (about 340–360 nm in the real size, due to scattered excitation) were excluded from analysis.

Parameters of Vesicle Motions (Mean ± SD)	Long-Distance Motions	Short-Distance Motions
Mean velocity (μm/s)	1.93 ± 0.05	1.09 ± 0.02
Maximum velocity (μm/s)	5.85	3.5
Minimal velocity (μm/s)	0.038	0.0081
Path length (μm/10 s)	11.5 ± 0.8	7.79 ± 1.2

long-distance motions, D^2 ranged from 2.1×10^{-2} $\mu m^2/s$ to 0.62 $\mu m^2/s$, with an average value of 0.11 ± 0.07 $\mu m^2/s$ ($n = 30$ vesicles). For short-distance motions, D^2 ranged from 8×10^{-3} $\mu m^2/s$ to 0.12 $\mu m^2/s$, with an average value of 5.3×10^{-2} $\mu m^2/s$ ($n = 30$ vesicles).

Quantifying Individual Secretory Vesicle Motions in Living Pollen Tubes

Much variation in velocity was observed during the recording time. In the pollen tubes observed for long periods, single secretory vesicles occasionally traveled distances of 100 μm at a top speed of 6.87 μm/s (in one instance), but such cases were rare (less than one vesicle per cell per minute) and were therefore excluded from further analysis. During pauses between directed runs, complex, oscillatory behaviors were observed. As shown in Figure 3A, oscillations occurred preferentially during pauses and before direction reversals. The average oscillation frequency was $\omega_{osc} = 0.34 \pm 0.08$ per second ($n = 12$ vesicles).

Exocytosis, the release material from secretory vesicles, was identifiable as a sudden spread of fluorescence. Exocytosis of a vesicle was preceded by a transient brightening of the vesicle followed by a decay of its fluorescence intensity (Fig. 3B), with a characteristic time of 13.7 ± 1.3 s ($n = 20$ pollen tubes). Fusion of vesicles appeared as a fluorescent spot spreading away from the site of fusion (Fig. 3C). The trace showed apparently random motion, superimposed with a slow drift. The trajectories were constrained in an irregular-shaped value of 1 μm in the x to y direction (Fig. 3D). For analysis, we measured the square of the distance traveled by the vesicles and plotted the MSD against the time interval (Fig. 3E). Table II summarizes the tracking parameters and other findings, as well as the ratios of vesicles with different motions in relation to all vesicles.

Effect of Actin Cytoskeleton Disruption on Secretory Vesicle Mobility

Disruption of the actin cytoskeleton by treatment with latrunculin B (LATB) or cytochalasin D (CD) caused significant alterations in secretory vesicle motions (Table III). The average vesicle path lengths in pollen tubes treated with LATB or CD was reduced to 7.34 ± 1.51 or 9.16 ± 1.37 μm of displacement per 10 s, respectively. These values represent significantly shorter path lengths than those measured in control cells (Fig. 4A). LATB treatment dramatically reduced the vesicle velocity as well; the velocity ranged from 0.20 to 0.96 μm/s, with an average velocity of 0.62 ± 0.21 μm/s, which is about one-fourth that observed in the control pollen tubes. CD showed similar but less significant effect on the velocity, reducing it to 0.65 to 1.04 μm/s, with an average value of 0.81 ± 0.09 μm/s (Fig. 4B). The alterations in vesicle trajectories caused by LATB and CD treatment were characterized by plotting the x-y coordinates of vesicles in the two experimental conditions. The results showed that long-distance motion occurred only in the untreated cells that had intact actin cytoskeletons (Supplemental Fig. 1A). Vesicles were much less mobile in the presence of both inhibitors (Supplemental Fig. 1, B and C), and their motions became random and were mostly confined to the restricted regions (Supplemental Fig. 1, G and H). Complex dynamics, such as the oscillations, regularly visualized in the control pollen tubes, were not observed in the LATB- and CD-treated pollen tubes (Fig. 4, C and D). Furthermore, the MSD curves (Fig. 4E) revealed that individual vesicle kinetics was clearly affected by these inhibitors, which reduced D^2 by 70% (Fig. 4F).

Effects of Microtubule Disruption on Secretory Vesicle Mobility

Microtubule disruption by treatment with the inhibitors oryzalin and colchicine led to more moderate alterations in secretory vesicle motion than did by actin cytoskeleton disruption. Incubation for 10 min with 100 μM oryzalin and 5 mM colchicine induced a 10% to 20% reduction in vesicle mobility (Supplemental Fig. 1, D and E). Vesicle tracking showed a clear reduction in vesicle mobility as detected in the x-y plane; the average path lengths were 9.91 and 10.6 μm in 10 s for oryzalin and colchicines, respectively, which represent approximately 80% of the mobility found near the plasma membrane in control cells (Fig. 4A). When traces of individual vesicle motions in control pollen tubes were compared to those in oryzalin- and colchicine-treated cells, a marked difference in velocity was noted (Fig. 4B). In addition, both oryzalin and colchicine treatments had a significant impact on vesicle trajectories, which were much more confined in the lateral directions than those of the control cells (Supplemental Fig. 1, I and J). Plots of MSD versus time revealed that vesicle motions in treated pollen tubes had a number of different, distinctive features, which deviated from the regulated motions observed in control pollen tubes. The averaged MSD plots are shown in Figure 4E. When pollen tubes were exposed to colchicine and oryzalin for 10 min, D^2 of mobile vesicles was reduced by only 25% to 40% (Fig. 4F).

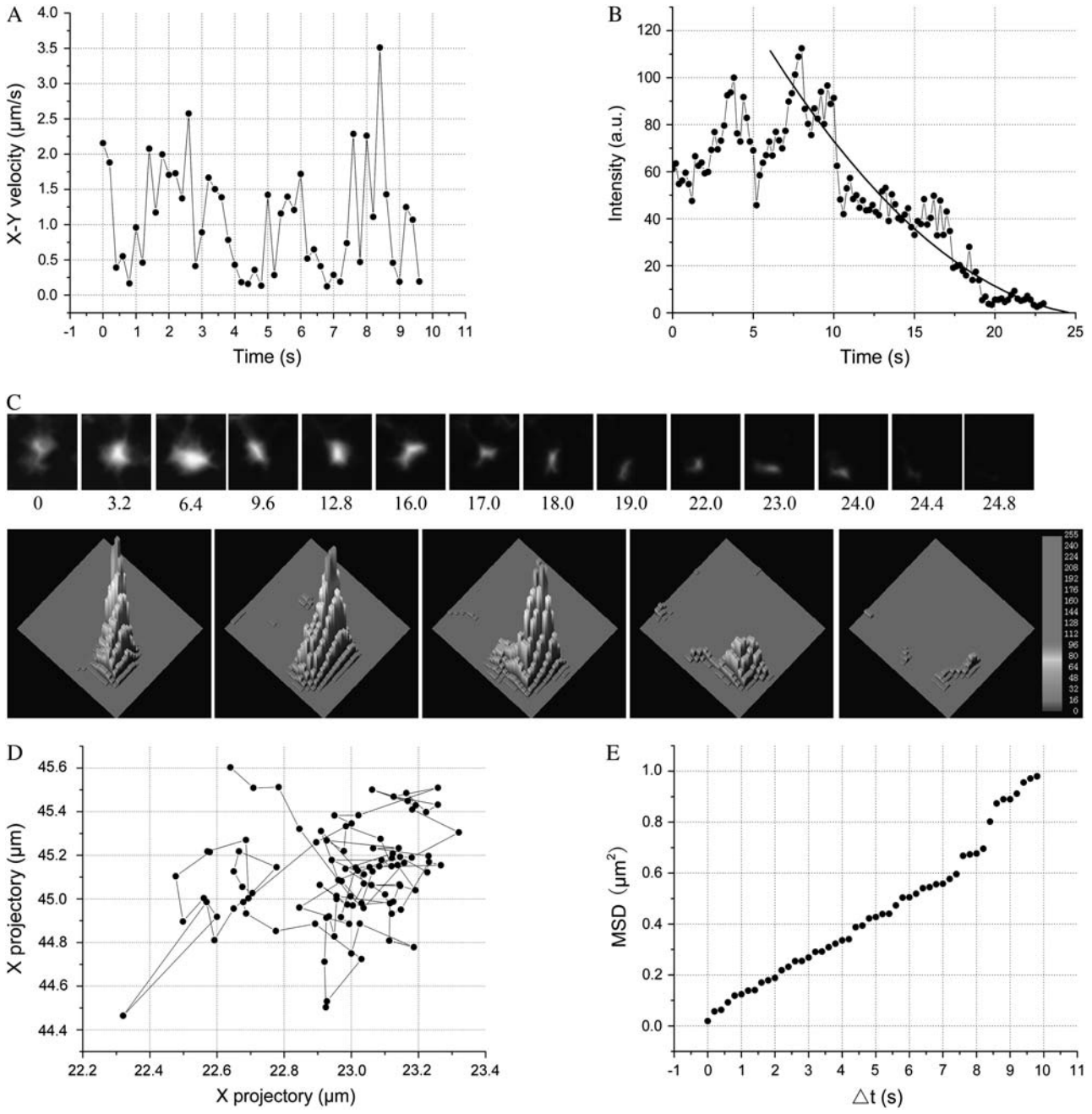

Figure 3. Trajectory of an individual secretory vesicle near the plasma membrane in living pollen tubes. A, Vesicle oscillation. Plot of the *x*-*y* velocity of an oscillating vesicle as a function of time (oscillation frequency ω_{osc} = 0.6 per second) is shown. B, Time course of the fluorescence intensity of the vesicle shown in A. The characteristic decay time of the fluorescence is given by a polynomial fit (black line): $t = 13.7 \pm 1.3$ s. C, Individual exocytotic events of a FM4-64-labeled vesicle. Numbers indicate time (in seconds) relative to the moment of fusion. Lower sections show three-dimensional luminance plots of four successive frames starting one frame before fusion. D, Lateral mobility of a vesicle on a plot of *x* versus *y* coordinates. E, MSD of an exocytotic vesicle plotted against time interval Δt.

Tracking parameters of secretory vesicles in treated pollen tubes are summarized in Table IV.

Effects of Brefeldin A on Secretory Vesicle Trafficking

We also characterized the effect of brefeldin A (BFA) on the mobility of secretory vesicle in living pollen tubes. When the pollen tubes were observed after a 10-min incubation with BFA, the average path lengths in apical and subapical regions were found to be slightly shorter than the average path lengths measured in control cells. The average path lengths for the apical and subapical regions in BFA-treated pollen tubes were 11.76 ± 2.35 μm and 9.42 ± 1.17 μm of

Table II. *Overview of individual secretory vesicle tracking parameters on the basis of 200 vesicles observed under EWM in five living pollen tubes*

N.D., Not defined. D^2, Derived from the slope of a plot of the MSD versus time for $\Delta t \rightarrow 0$.

Vesicle Tracking Parameters (Mean ± SD)	Long-Distance Motions	Short-Distance Motions	Exocytotic Vesicles
Proportion (%)	Approximately 8%	Approximately 90%	<1%
Area density ($1/\mu m^2$)	0.011 ± 0.008	0.038 ± 0.007	N.D.
Total path length (μm/10 s)	16.5 ± 0.9	7.8 ± 1.2	10.4 ± 0.8
Mean velocity (μm/s)	1.5 ± 0.4	0.8 ± 0.3	0.9 ± 0.4
D^2 (μm^2/s)	0.11 ± 0.07	0.053 ± 0.04	0.065 ± 0.03

displacement per 10 s, respectively (Fig. 5A). The velocities of the mobile vesicles varied, but they were generally comparable to those of vesicles in the control pollen tubes. The average velocity of vesicles in the subapical region was 1.87 ± 0.15 μm/s, and the maximum velocity was 3.26 μm/s. The velocity of vesicles in the apical region often decreased to an average value of 0.95 ± 0.34 μm/s (Fig. 5B) when they were moving closer toward the plasma membrane. The *x-y* coordinates of vesicles in the treated pollen tube are plotted (Supplemental Fig. 1F), which illustrates that BFA treatment had a minimal effect on vesicle trajectories. Nevertheless, oscillations of secretory vesicles in pollen tubes did not disappear upon treatment with BFA (Fig. 5C). As shown in Figure 5D, the MSD curve of individual vesicles in the pollen tubes after BFA treatment was not significantly influenced. D^2 values deduced from the MSD curves were reduced by nearly 10% by BFA treatment (Fig. 5E). In BFA-treated pollen tubes, about 30 to 40 vesicles were visible in the observation field, corresponding to average densities of $1.4 \times 10^{-2} \pm 0.003$ μm^{-2} and $2.3 \times 10^{-2} \pm 0.002$ μm^{-2} in the subapical and apical regions, respectively (Fig. 5F). The total number of visible secretory vesicles decreased after BFA treatment, suggesting that the supply of new secretory vesicles to the observed regions was disrupted.

DISCUSSION

Imaging techniques are powerful tools for detecting vesicle trafficking in living cells, and they can provide information concerning the mechanisms of vesicle trafficking (Betz and Angleson, 1998; Fletcher et al., 2000; Baumann et al., 2005). Because confocal microscopy provides excellent optical sectioning, it has been widely used in the investigation of endocytosis and exocytosis in living cells (Ohara-Imaizumi et al., 2002; Bolte et al., 2004; Ma et al., 2004; Šamaj, 2006). However, vesicle diameters in pollen tubes range from 75 to 200 nm (Derksen et al., 1995), and, thus, vesicles are beyond the resolution limits of a conventional confocal microscope. In this study, we used a high numerical aperture objective and varied the angle of incidence of the laser beam to generate a penetration depth of the evanescent field of 70 to 400 nm proximal to the plasma membrane with cells adhered to a glass coverslip. EWM has provided valuable and complementary information about vesicle trafficking, especially in living cells, under lengthy observation periods (Watkins and Robertson, 1977; Oheim et al., 1999). In terms of depth discrimination, an evanescent wave microscope is up to 10-fold better than a confocal microscope (Steyer and Almers, 2001). Combined with a high-resolution charge-coupled device, which has extremely high temporal sensitivity, EWM is very useful in tracking 2-D motions of small particles near the coverslip under physiological conditions (Steyer et al., 1997; Sund et al., 1999; Sund and Axelrod, 2000; Wiegand et al., 2002; Mashanov et al., 2003; Ohara-Imaizumi et al., 2004; Xia et al., 2004; Zenisek et al., 2004). In this report, we examined the dynamics and motions of FM4-64-labeled vesicles proximal to the plasma membrane in living pollen tubes of *P. meyeri*. To our knowledge, this report is the first description of visualization of secretory vesicle tracking in living pollen tubes using EWM. This technique greatly facilitates the quantification of vesicle trafficking in plant cells.

Pollen tubes have been used as in vivo model systems for studying vesicles and organelle tracking because they are highly polarized, tip growing, and easy to manipulate experimentally. Angiosperm pollen tubes have been chosen as the subjects of most previous investigations because they grow quickly. For example, the growth rate of *Lilium longiflorum* was reported to be about 5 to 25 μm/min (Parton et al., 2001). In our study, we used the slow-growing pollen tubes of *P. meyeri*, which have a growth rate of 20 μm/h (Anderhag et al., 2000), so that we could easily follow the secretory vesicle motion. Our current understanding of vesicle trafficking in pollen tubes is based primarily on ultrastructural studies and mathematical modeling of vesicle trafficking in relation to tip growth (Derksen et al., 1995; Ketelaar, 2002). Lancelle and Hepler (1992) defined an apical clear zone as a vesicular

Table III. *Disruption of the actin cytoskeleton reduced the secretory vesicle mobility (n = 30 pollen tubes)*

Parameter of Vesicle Motions (Mean ± SD)	10 nM LATB	10 μM CD
Mean velocity (μm/s)	0.62 ± 0.21	0.81 ± 0.09
Maximum velocity (μm/s)	0.65	1.04
Minimal velocity (μm/s)	0.20	0.96
Path length (μm/10 s)	7.34 ± 1.51	9.16 ± 1.37
D^2 (μm^2/s)	0.042 ± 0.021	0.049 ± 0.013

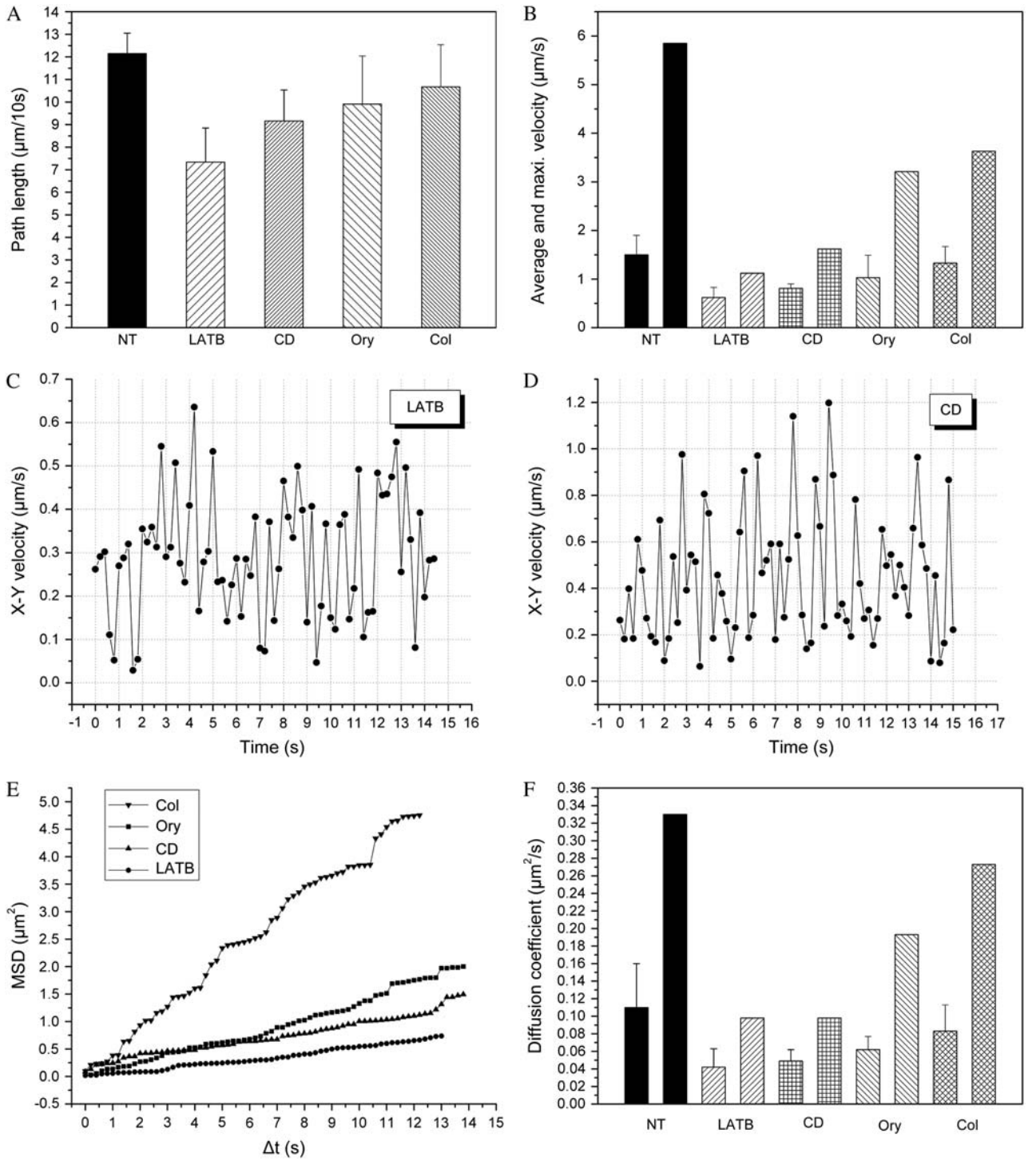

Figure 4. Effects of cytoskeleton disruption on mobility of secretory vesicles. A, The average path lengths of vesicles of the nontreated (NT), LATB-treated (LATB), CD-treated (CD), oryzalin-treated (Ory), and colchicine-treated (Col) pollen tubes (n = 12). B, Bar graph depicting the mean and maximum velocities of vesicles in NT, LATB-, CD-, Ory-, and Col-treated pollen tubes (n = 12). C, Plot of the x-y velocity of an individual vesicle in a LATB-treated pollen tube. D, Plot of the x-y velocity of an individual vesicle in a CD-treated pollen tube. E, MSD of vesicle motions in LATB-, CD-, Ory-, and Col-treated pollen tubes plotted against time interval Δt. To calculate the MSD, we measured the distance moved over an interval of fixed duration (0.2 s), with the interval starting first at 0 ms after the beginning of the recording, then at 200 ms, at 400 ms, and so on until at 13 s. F, Calculated 2-D diffusion coefficient of vesicle motions, D^2, of the NT, LATB-, CD-, Ory-, and Col-treated pollen tubes.

Table IV. *Characteristics of secretory vesicle mobility in pollen tubes with disrupted microtubules (n = 12 pollen tubes)*

Parameter of Vesicle Motions (Mean ± SD)	100 μM Oryzalin	5 mM Colchicine
Mean velocity (μm/s)	1.03 ± 0.46	1.33 ± 0.34
Maximum velocity (μm/s)	3.21	3.63
Minimal velocity (μm/s)	0.47	0.55
Path length (μm/10 s)	9.91	10.6
D^2 (μm^2/s)	0.062 ± 0.041	0.083 ± 0.053

zone depleted of organelles that is located in the apical region of *L. longiflorum* pollen tubes using TEM, and Parton et al. (2001) used FM4-64 and confocal microscopy to reveal that the apical clear zone is a vesicle-rich, V-shaped region at the apex of *L. longiflorum* pollen tubes. In our study, however, we found that in gymnosperm the staining pattern at the tube apex did not correspond spatially to the previously described V-shaped, apical clear zone containing secretory vesicles, confirming that the cytoplasmic organization of gymnosperm pollen tubes was distinct from that of angiosperm pollen tubes (Justus et al., 2004; Wang et al., 2005; Chen et al., 2006).

In previous studies, some organelles moved linearly, in a mostly circulatory pattern (Cai et al., 2001), whereas the majority of organelles in *Pinus sylvestris* pollen tubes exhibited Brownian-like motions (Terasaka and Niitsu, 1994; de Win et al., 1996). The experiments described herein clearly show that vesicles were significantly held back when they moved, and that two classes of secretory vesicle motions are present. Most of the motions are short distance. Furthermore, we found that the tracks of vesicle motions were longer and straighter in the center than in the peripheral portions, and that vesicles moved more slowly at the apical regions than in the middle and subapical regions. Using a pharmacological approach with the actin-disrupting drugs LATB and CD, we confirmed that the intact actin cytoskeleton was essential for secretory vesicle transport in pollen tubes. Indeed, this notion is supported by recent data showing that actin-dependent motions of FYVE (Fab-1, YGL023, Vps27, and EEA1)-labeled endosomes within the clear zone are essential for the tip growth of root hairs (Voigt et al., 2005; Šamaj, 2006), and that active F-actin gels drive shape oscillations in animal cells and their cell fragments (Paluch et al., 2005).

In our investigations, we observed that exocytotic vesicles entered the evanescent field and then became brighter, losing their lateral mobility while they reached a stable maximum intensity, and then their intensity declined as the dye diffused away. From the spread of fluorescence of secretory vesicles, we deduced that exocytosis is a "full" fusion event involving collapse of the vesicles into the membrane as they release of their internal components. The fusion event in living pollen tubes was not consistent with the "kiss-and-run" model recently reported in synapses (Gandhi and Stevens, 2003; Wightman and Haynes, 2004), indicating that the mechanism of vesicle fusion events in plant cells differs from that of animal cells.

One of the most intriguing aspects of pollen tube growth is the phenomenon of periodicity or oscillation in growth rate (Pierson et al., 1996; Messerli et al., 2000; Holdaway-Clarke et al., 2003). In our study, complex dynamics, including oscillations, were observed in living pollen tubes. Both long- and short-distance motions exhibited this complicated behavior, and the oscillation frequency of short-distance motions was higher than that of long-distance motions. Given the link between growth rate and oscillatory vesicle motions, our data indicate that the underlying periodicity in the pollen tubes is dependent on vesicle secretion and apical extension normally associated with growth. In addition, the MSD plots yielded sigmoidal, irregular curves. In the case that vesicles move randomly and with a single diffusion coefficient, the plot should yield straight lines with slopes proportional to the diffusion coefficients. According to Stokes' law, a sphere should diffuse at $D^2 = 2.43\ \mu m^2/s$ in an aqueous medium, assuming an average diameter of 200 nm. However, D^2 of vesicles in *P. meyeri* pollen tubes deduced from the plots was $3.23 \times 10^{-2} \pm 0.0092$, or about 1/100th of the estimate for free aqueous diffusion. Therefore, we concluded that the motions of vesicles in the living pollen tubes were neither random nor Brownian.

Animal cell studies have largely focused on the role of the actin cytoskeleton in vesicle trafficking (Merrifield et al., 1999; Jerdeva et al., 2005; Yarar et al., 2005), but some researchers have suggested a possible role for microtubules as well (Elkjaer et al., 1995; Hamm-Alvarez and Sheetz, 1998; Araki, 2006). In various plant cell types, most intracellular mobility seems to occur along actin cables (hyphae: Torralba et al., 1998; pollen tubes: Parton et al., 2003; Justus et al., 2004; root hairs: Tominaga et al., 1997; Voigt et al., 2005; Šamaj, 2006). Actin cytoskeleton and microtubules are coaligned in a longitudinal array that extends from the amyloplasts into the base of the clear zone (Lazzaro, 1999; Anderhag et al., 2000; Parton et al., 2003), which is the specific region where vesicles were observed and large organelles were nearly absent. However, less is understood about the role of microtubules and their interactions with the actin cytoskeleton in regulating vesicle motion and transport. In this study, the characteristically high mobility of vesicles changed drastically after treatment with actin inhibitors, such that most of the observed vesicles remained in restricted regions during the observation periods. The marked effects of these agents on vesicle motion kinetics suggest that actin cytoskeletons play a primary role in secretory vesicle mobility throughout the cytoplasm of the entire pollen tube. Given the properties of actin oscillation and self-organization in eukaryotic cells (Vicker, 2000, 2002), we concluded that the actin dynamics fundamentally determined the vesicle oscillation in living pollen tubes. However, microtubule inhibitors also showed, albeit less dramatic, effects on vesicle mobility. A possible scenario is that microtubules function as organizing elements, maintaining

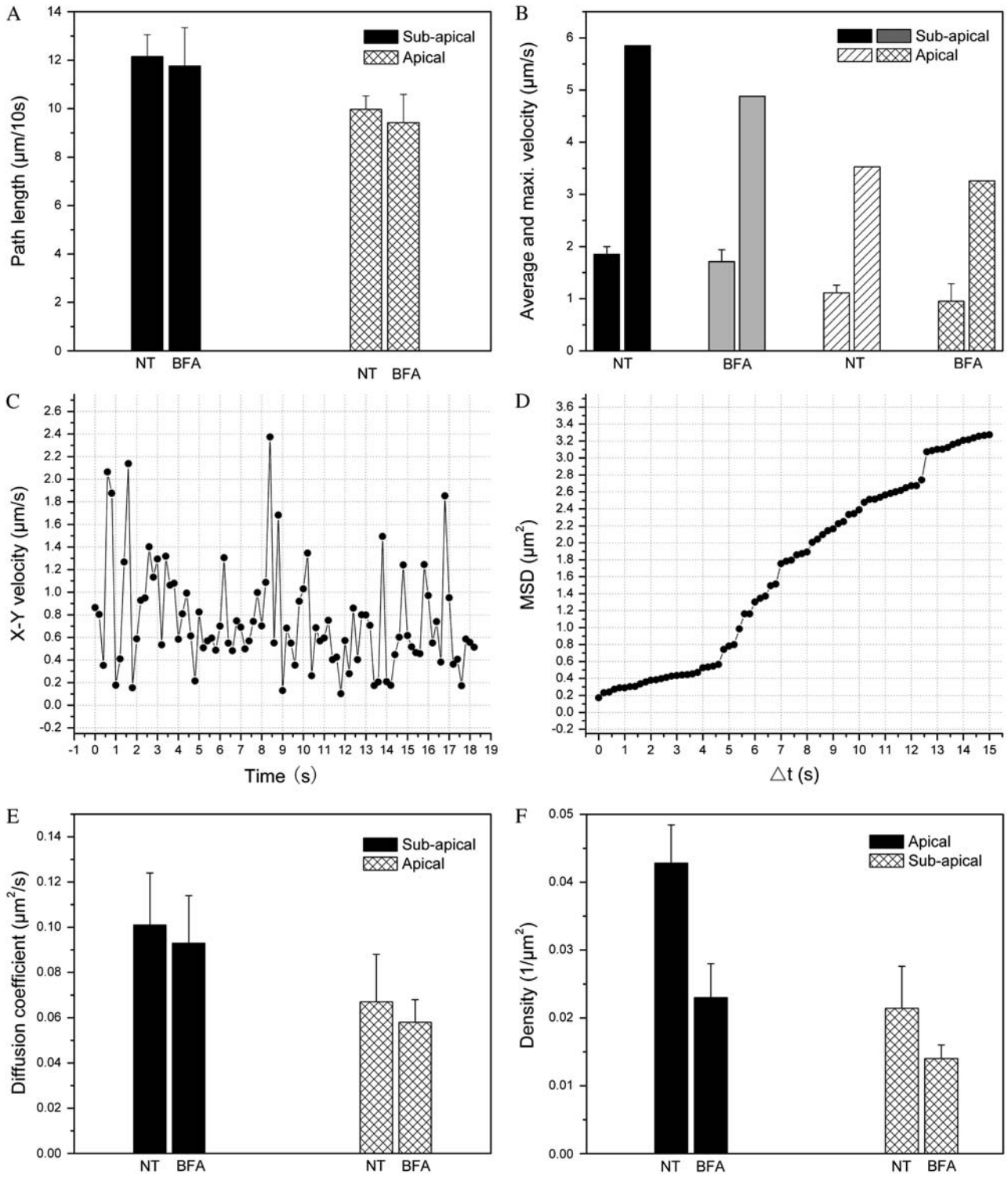

Figure 5. BFA-induced changes in dynamics of secretory vesicles in living pollen tubes. A, Histograms depicting the average path lengths in apical and subapical regions after 10 min of BFA treatment ($n = 8$). B, Bar graph depicting the average and maximum velocities of vesicles with or without BFA treatment. C, The plot of *x-y* velocity of an individual vesicle in a BFA-treated pollen tube. D, MSD of vesicle motion in a BFA-treated pollen tube. MSD was calculated as a function of the observation time. E, Data from vesicle motions in BFA-treated and control pollen tubes were pooled to calculate the 2-D diffusion coefficient D^2. F, The average vesicle density changed in BFA-treated pollen tubes.

the actin cytoskeleton in an intact state, so that disruption of the microtubules indirectly alters vesicle mobility. Therefore, we can safely conclude that the actin cytoskeleton is the main underlying mechanism for vesicle mobility and that microtubules within the elongating pollen tube influence microfilament organization, thus affecting the mobility of vesicles.

The fungal metabolite BFA has been widely used as a useful tool in studies of the relationship between membrane trafficking and secretion. It has been reported as inhibiting vesicle coat formation, blocking endoplasmic reticulum-to-Golgi trafficking, and disrupting the Golgi apparatus (Donaldson et al., 1992; Yasuhara et al., 1995; Robineau et al., 2000; Wang et al., 2005). Interestingly, more recent evidence indicates that BFA affects both actin organization and actin-dependent endosomal mobility within the growing tips of root hairs (Šamaj et al., 2002; Voigt et al., 2005). The experiments described herein indicate that BFA causes a significant decrease in vesicle density in both the apical and subapical regions, probably as a result of its inhibitory effect on the production of secretory vesicles. Furthermore, we observed a trend of decreasing vesicle velocity and mobility in pollen tubes after treatment with BFA. Although the effect was not significant, in light of the role of the actin cytoskeleton in regulating vesicle trafficking, the reduction in vesicle mobility may be interpreted as a direct consequence of the BFA-induced modification of the actin cytoskeleton. Taken together, our experiments indicate that in *P. meyeri* pollen tubes, BFA affects secretory vesicle formation more than it affects vesicle mobility.

In summary, a fluorescence excitation technique using variable penetration depths of evanescent waves was modified and applied to investigations of secretory vesicles trafficking in living *P. meyeri* pollen tubes. The secretory vesicles were labeled with the membrane-specific dye FM4-64. Using EWM, we observed exocytosis of secretory vesicles via a ''full'' fusion event, and we found that there were two types of vesicle motions showing different oscillation frequencies. Contrary to earlier investigations using confocal microscopy, our results indicate that secretory vesicle motions in living pollen tubes are not Brownian, and they are dependent on the actin cytoskeleton. In addition, BFA prominently inhibits vesicle formation, but not vesicle mobility, in living pollen tubes. EWM can be used not only as an independent assay for vesicle trafficking, but also as a new, powerful tool for studies on the dynamics of vesicles, organelles, and single molecules of plant cells, which may now be undertaken in much more detail than ever before.

MATERIALS AND METHODS

Plant Materials

Cones with mature pollen were collected from *Picea meyeri* Rehd. et Wils growing in the Botanical Garden of the Institute of Botany, Chinese Academy of Sciences, prior to the beginning of the pollination season in mid-April 2004. Cones were dried overnight at room temperature, and the dry pollen was stored at −20°C until further use.

Pollen Culture

Stored pollen was equilibrated at room temperature for 30 min and then carefully suspended in a culture medium (2 mg of pollen per mL medium) that contained 12% (w/v) Suc, 0.03% calcium chloride, and 0.01% boric acid in a shaker at 100 rpm. The pH of the medium was adjusted to 6.4 with phosphate buffered saline. Germination took place in the dark at 25°C.

Dye Labeling

FM4-64 dye was purchased from Sigma. In this experiment, loading of cells with FM4-64 dye was generally achieved by application at a concentration of 2 μM during the imbibition of pollen tubes by direct addition of dye solutions in the culture medium. After 5 min of loading with FM4-64, the medium containing dye was replaced with fresh medium lacking the dye.

Drug Treatment

Inhibitor stock solutions were made up in 100% ethanol (2 mM CD, 20 mM oryzalin, 50 mM colchicine, and 5 mg/mL BFA), except for LATB, which was a 1 mM stock in dimethyl sulfoxide. All of the inhibitors were purchased from Sigma. The final inhibitor concentrations in the germination media were up to 10 μM for CD, 10 nM for LATB, 100 μM for oryzalin, 5 mM for colchicine, and 5 μg/mL for BFA (Supplemental Fig. 2 shows the appropriate concentrations we selected). Actin cytoskeletons were disrupted using 10 nM LATB or 10 μM CD for 10 min after labeling with FM4-64 at 25°C, respectively. The microtubule was disrupted by incubating pollen tubes with 100 μM oryzalin or 5 mM colchicine for 10 min after labeling with FM4-64 at 25°C. BFA was applied together with FM dyes at a concentration of 5 μg/mL.

Confocal Microscope Imaging

Sorbitol (100 μM) and sodium azide (500 μM) were applied directly to the medium. The pollen tubes were examined and digital images were acquired using a laser scanning confocal system installed on an inverted microscope (IX81; Olympus). The samples were excited at 514 nm with a 30-mW argon ion laser operated at full power at an intensity of 3%, achieved by means of neutral-density filters, with a nearly closed pinhole and the gain adjusted to below 7.00. Emission was detected with a 530- to 600-nm band-path filter (Zeiss R510; Carl Zeiss). Images were collected and processed using Adobe Photoshop 7.0 (Adobe Systems).

EWM

The total internal reflection system was constructed based on an inverted microscope (IX81; Olympus). Light from a multichannel argon laser (458, 488, 515 nm; 30 mW) was introduced to the microscope through a single-mode fiber and three illumination lenses. The light was focused at the back focal plane of a high aperture objective lens (Apo 100× OHR; NA 1.65; Olympus). This allowed us to generate evanescent waves with penetration depths from approximately 60 to 400 nm in aqueous solution ($n = 1.33$) at an excitation wavelength of 515 nm laser. FM4-64-labeled cells were visualized by excitation with an argon laser set to 514 nm. Emission was detected with a 530- to 600-nm band-path filter (Zeiss R510; Carl Zeiss).

Evanescent Wave Microscope Imaging Collection and Analysis

Fluorescence was gathered through a 100× Apo OHR objective (NA 1.65; Olympus), and the evanescent wave microscope images were captured through the right lateral port of the inverted microscope onto a cooled charge-coupled device camera (Micromax, MMX-512-BFT; Princeton Instruments), which was operated with Metamorph 6.0 (Universal Imaging). Immersion oil with a high refractive index ($n = 1.65$) was used to bridge the optical contact between the objective and the cover glass, and the incident light for evanescent illumination was introduced from the objective lens. Time-lapse images were acquired every 200 ms and sampled into the computer through a frame grabber with genuine 16 Bit (2^{16}; 65,536 gray levels).

Image analysis was performed with Image-Pro Plus 5.1 (Media Cybernetics), Adobe Photoshop 7.0 (Adobe Systems), and ImageJ 1.34e (Wayne Rasband, National Institutes of Health). The raw images were filtered to enhance the visibility of the vesicles. A high-pass fast Fourier transform filter, followed by a 3- × 3-pixel trimmed mean filter, was applied to remove nonuniform background noise, and a flatten filter was used to smooth the background. The pixel size was 0.125 μm with a 1.6× optical zoom, and the image size was typically 326 × 484 pixels. The fluorescence intensity was expressed in the 8-bit value of digitization as described previously (Tsuboi et al., 2000; Taraska and Almers, 2004).

ACKNOWLEDGMENTS

We thank Dr. Richard Turner, Dr. Mathem Benson, and Prof. Yuxi Hu for valuable discussion at the early stages of these experiments, and Dr. Bai Li for technical assistance with EWM. We also thank Dr. Lingan Kong for his valuable comments on an early draft of this manuscript.

Received March 15, 2006; revised June 6, 2006; accepted June 8, 2006; published June 23, 2006.

LITERATURE CITED

Anderhag P, Hepler P, Lazzaro M (2000) Microtubules and microfilaments are both responsible for pollen tube elongation in the conifer *Picea abies* (Norway spruce). Protoplasma **214:** 141–157

Araki N (2006) Role of microtubules and myosins in Fc gamma receptor-mediated phagocytosis. Front Biosci **11:** 1479–1490

Baumann NA, Sullivan DP, Ohvo-Rekila H, Simonot C, Pottekat A, Klaassen Z, Beh CT, Menon AK (2005) Transport of newly synthesized sterol to the sterol-enriched plasma membrane occurs via nonvesicular equilibration. Biochemistry **44:** 5816–5826

Betz WJ, Angleson JK (1998) The synaptic vesicle cycle. Annu Rev Physiol **60:** 347–363

Bolte S, Talbot C, Boutte Y, Catrice O, Read ND, Satiat-Jeunemaitre B (2004) FM-dyes as experimental probes for dissecting vesicle trafficking in living plant cells. J Microsc **214:** 159–173

Bretscher MS, Aguado-Velasco C (1998) Membrane traffic during cell locomotion. Curr Opin Cell Biol **10:** 537–541

Cai G, Romagnoli S, Cresti M (2001) Microtubule motor proteins and the organization of the pollen tube cytoplasm. Sex Plant Reprod **14:** 27–34

Chen Y, Chen T, Shen S, Zheng M, Guo Y, Lin J, Baluška F, Šamaj J (2006) Differential display proteomic analysis of Picea meyeri pollen germination and pollen tube growth after actin depolymerization by latrunculin B. Plant J **47:** 194–195

de Win AHN, Knuiman B, Pierson ES, Geurts H, Kengen HMP, Derksen J (1996) Development and cellular organization of *Pinus sylvestris* pollen tubes. Sex Plant Reprod **9:** 93–101

de Win AHN, Pierson ES, Timmer C, Lichtscheidl IK, Derksen J (1998) Interactive computer-assisted position acquisition procedure designed for the analysis of organelle movement in pollen tubes. Cytometry **32:** 263–267

Derksen J, Rutten T, Lichtscheidl IK, de Win AHN, Pierson ES, Rongen G (1995) Quantitative analysis of the distribution of organelles in tobacco pollen tubes: implications for exocytosis and endocytosis. Protoplasma **188:** 267–276

Dettmer J, Hong-Hermesdorf A, Stierhof Y-D, Schumacher K (2006) Vacuolar H^+-ATPase activity is required for endocytic and secretory trafficking in Arabidopsis. Plant Cell **18:** 715–730

Donaldson JG, Cassel D, Kahn RA, Klausner RD (1992) ADP-ribosylation factor, a small GTP-binding protein, is required for binding of the coatomer protein beta-COP to Golgi membranes. Proc Natl Acad Sci USA **89:** 6408–6412

Elkjaer ML, Birn H, Agre P, Christensen EI, Nielsen S (1995) Effects of microtubule disruption on endocytosis, membrane recycling and polarized distribution of Aquaporin-1 and gp330 in proximal tubule cells. Eur J Cell Biol **67:** 57–72

Emons AM, Mulder BM (2000) How the deposition of cellulose microfibrils builds cell wall architecture. Trends Plant Sci **5:** 35–40

Fischer-Parton S, Parton RM, Hickey P, Dijksterhuis J, Atkinson HA, Read ND (2000) Confocal microscopy of FM4-64 as a tool for analysing endocytosis and vesicle trafficking in living fungal hyphae. J Microsc **198:** 246–259

Fletcher LM, Welsh GI, Oatey PB, Tavare JM (2000) Role for the microtubule cytoskeleton in GLUT4 vesicle trafficking and in the regulation of insulin-stimulated glucose uptake. Biochem J **352:** 267–276

Foissner I, Lichtscheidl IK, Wasteneys GO (1996) Actin-based vesicle dynamics and exocytosis during wound wall formation in characean internodal cells. Cell Motil Cytoskeleton **35:** 35–48

Gandhi SP, Stevens CF (2003) Three modes of synaptic vesicular recycling revealed by single-vesicle imaging. Nature **423:** 607–613

Hamm-Alvarez SF, Sheetz MP (1998) Microtubule-dependent vesicle transport: modulation of channel and transporter activity in liver and kidney. Physiol Rev **78:** 1109–1129

Hepler PK, Vidali L, Cheung AY (2001) Polarized cell growth in higher plants. Annu Rev Cell Dev Biol **17:** 159–187

Holdaway-Clarke TL, Weddle NM, Kim S, Robi A, Parris C, Kunkel JG, Hepler PK (2003) Effect of extracellular calcium, pH and borate on growth oscillations in *Lilium formosanum* pollen tubes. J Exp Bot **54:** 65–72

Jerdeva GV, Wu K, Yarber FA, Rhodes CJ, Kalman D, Schechter JE, Hamm-Alvarez SF (2005) Actin and non-muscle myosin II facilitate apical exocytosis of tear proteins in rabbit lacrimal acinar epithelial cells. J Cell Sci **118:** 4797–4812

Justus CD, Anderhag P, Goins JL, Lazzaro MD (2004) Microtubules and microfilaments coordinate to direct a fountain streaming pattern in elongating conifer pollen tube tips. Planta **219:** 103–109

Ketelaar T (2002) Spatial organisation of cell expansion by the cytoskeleton. PhD thesis. Wageningen University, Wageningen, The Netherlands

Kimura S, Laosinchai W, Itoh T, Cui X, Linder CR, Brown RM Jr (1999) Immunogold labeling of rosette terminal cellulose-synthesizing complexes in the vascular plant *vigna angularis.* Plant Cell **11:** 2075–2086

Kuhn JR, Pollard TD (2005) Real-time measurements of actin filament polymerization by total internal reflection fluorescence microscopy. Biophys J **88:** 1387–1402

Lancelle SA, Hepler PH (1992) Ultrastructure of freeze-substituted pollen tubes of *Lilium longiflorum.* Protoplasma **167:** 215–230

Lazzaro MD (1999) Microtubule organization in germinated pollen of the conifer *Picea abies* (Norway spruce, Pinaceae). Am J Bot **86:** 759–766

Ma L, Bindokas VP, Kuznetsov A, Rhodes C, Hays L, Edwardson JM, Ueda K, Steiner DF, Philipson LH (2004) Direct imaging shows that insulin granule exocytosis occurs by complete vesicle fusion. Proc Natl Acad Sci USA **101:** 9266–9271

Mashanov GI, Tacon D, Knight AE, Peckham M, Molloy JE (2003) Visualizing single molecules inside living cells using total internal reflection fluorescence microscopy. Methods **29:** 142–152

Merrifield CJ, Moss SE, Ballestrem C, Imhof BA, Giese G, Wunderlich I, Almers W (1999) Endocytic vesicles move at the tips of actin tails in cultured mast cells. Nat Cell Biol **1:** 72–74

Messerli MA, Creton R, Jaffe LF, Robinson KR (2000) Periodic increases in elongation rate precede increases in cytosolic Ca^{2+} during pollen tube growth. Dev Biol **222:** 84–98

Ohara-Imaizumi M, Nakamichi Y, Tanaka T, Katsuta H, Ishida H, Nagamatsu S (2002) Monitoring of exocytosis and endocytosis of insulin secretory granules in the pancreatic beta-cell line MIN6 using pH-sensitive green fluorescent protein (pHluorin) and confocal laser microscopy. Biochem J **363:** 73–80

Ohara-Imaizumi M, Nishiwaki C, Kikuta T, Kumakura K, Nakamichi Y, Nagamatsu S (2004) Site of docking and fusion of insulin secretory granules in live MIN6 beta cells analyzed by TAT-conjugated anti-syntaxin 1 antibody and total internal reflection fluorescence microscopy. J Biol Chem **279:** 8403–8408

Oheim M, Loerke D, Stuhmer W, Chow RH (1999) Multiple stimulation-dependent processes regulate the size of the releasable pool of vesicles. Eur Biophys J **28:** 91–101

Ovecka M, Lang I, Baluška F, Ismail A, Illeš P, Lichtscheidl I (2005) Endocytosis and vesicle trafficking during tip growth of root hairs. Protoplasma **226:** 39–54

Paluch E, Piel M, Prost J, Bornens M, Sykes C (2005) Cortical actomyosin breakage triggers shape oscillations in cells and cell fragments. Biophys J **89:** 724–733

Parton RM, Fischer-Parton S, Trewavas AJ, Watahiki MK (2003) Pollen tubes exhibit regular periodic membrane trafficking events in the absence of apical extension. J Cell Sci **116:** 2707–2719

Parton RM, Fischer-Parton S, Watahiki MK, Trewavas AJ (2001) Dynamics of the apical vesicle accumulation and the rate of growth are related in individual pollen tubes. J Cell Sci **114:** 2685–2695

Picton JM, Steer MW (1983) Membrane recycling and the control of secretory activity in pollen tubes. J Cell Sci **63:** 303–310

Pierson ES, Miller DD, Callaham DA, van Aken J, Hackett G, Hepler PK (1996) Tip-localized calcium entry fluctuates during pollen tube growth. Dev Biol **174:** 160–173

Robineau S, Chabre M, Antonny B (2000) Binding site of brefeldin A at the interface between small G protein ADP-ribosylation factor 1 (ARF1) and the nucleotide-exchange factor Sec7 domain. Proc Natl Acad Sci USA **97:** 9913–9918

Rothman JE (1994) Mechanisms of intracellular protein transport. Nature **372:** 55–63

Rutten TL, Knuiman B (1993) Brefeldin A effects on tobacco pollen tubes. Eur J Cell Biol **61:** 247–255

Rutter GA, Tsuboi T (2004) Kiss and run exocytosis of dense core secretory vesicles. Neuroreport **15:** 79–81

Šamaj J (2006) Methods and molecular tools for studying endocytosis in plants: an overview. *In* J Šamaj, F Baluška, D Menzel, eds, Plant Endocytosis. Springer, Heidelberg, pp 1–17

Šamaj J, Ovecka M, Hlavacka A, Lecourieux F, Meskiene I, Lichtscheidl I, Lenart P, Salaj J, Volkmann D, Bogre L, et al (2002) Involvement of the mitogen-activated protein kinase SIMK in regulation of root hair tip growth. EMBO J **21:** 3296–3306

Šamaj J, Read ND, Volkmann D, Menzel D, Baluska F (2005) The endocytic network in higher plants. Trends Cell Biol **15:** 425–433

Sieberer B, Emons AMC (2000) Cytoarchitecture and pattern of cytoplasmic streaming in root hairs of *Medicago truncatula* during development and deformation by nodulation factors. Protoplasma **214:** 118–127

Steyer JA, Almers W (2001) A real-time view of life within 100 nm of the plasma membrane. Nat Rev Mol Cell Biol **2:** 268–275

Steyer JA, Horstmann H, Almers W (1997) Transport, docking and exocytosis of single secretory granules in live chromaffin cells. Nature **388:** 474–478

Sudhof TC (2004) The synaptic vesicle cycle. Annu Rev Neurosci **27:** 509–547

Sund SE, Axelrod D (2000) Actin dynamics at the living cell submembrane imaged by total internal reflection fluorescence photobleaching. Biophys J **79:** 1655–1669

Sund SE, Swanson JA, Axelrod D (1999) Cell membrane orientation visualized by polarized total internal reflection fluorescence. Biophys J **77:** 2266–2283

Taraska JW, Almers W (2004) Bilayers merge even when exocytosis is transient. Proc Natl Acad Sci USA **101:** 8780–8785

Terasaka O, Niitsu T (1994) Differential roles of microtubule and actin-myosin cytoskeleton in the growth of *Pinus* pollen tubes. Sex Plant Reprod **7:** 264–272

Tominaga M, Morita K, Sonobe S, Yokota E, Shimmen T (1997) Microtubules regulate the organization of actin filaments at the cortical region in root hairs of *Hydrocharis*. Protoplasma **199:** 83–92

Torralba S, Raudaskoski M, Pedregosa AM (1998) Effects of methyl benzimidazole-2-yl carbamate on microtubule and actin cytoskeleton in *Aspergillus nidulans*. Protoplasma **202:** 54–64

Tsuboi T, Rutter GA (2003) Insulin secretion by 'kiss-and-run' exocytosis in clonal pancreatic islet beta-cells. Biochem Soc Trans **31:** 833–836

Tsuboi T, Zhao C, Terakawa S, Rutter GA (2000) Simultaneous evanescent wave imaging of insulin vesicle membrane and cargo during a single exocytotic event. Curr Biol **10:** 1307–1310

Vicker MG (2000) Reaction-diffusion waves of actin filament polymerization/depolymerization in *Dictyostelium pseudopodium* extension and cell locomotion. Biophys Chem **84:** 87–98

Vicker MG (2002) Eukaryotic cell locomotion depends on the propagation of self-organized reaction-diffusion waves and oscillations of actin filament assembly. Exp Cell Res **275:** 54–66

Vo YP, Hutton JC, Angleson JK (2004) Recycling of the dense-core vesicle membrane protein phogrin in Min6 beta-cells. Biochem Biophys Res Commun **324:** 1004–1010

Voigt B, Timmers A, Šamaj J, Hlavacka A, Ueda T, Preuss M, Nielsen E, Mathur J, Emans N, Stenmark H, et al (2005) Actin-propelled motility of endosomes is tightly linked to polar tip-growth of root hairs. Eur J Cell Biol **84:** 609–621

Wang D, Quick MW (2005) Trafficking of the plasma membrane gamma-aminobutyric acid transporter GAT1. Size and rates of an acutely recycling pool. J Biol Chem **280:** 18703–18709

Wang Q, Kong L, Hao H, Wang X, Lin J, Samaj J, Baluska F (2005) Effects of brefeldin A on pollen germination and tube growth. Antagonistic effects on endocytosis and secretion. Plant Physiol **139:** 1692–1703

Watkins RW, Robertson CR (1977) A total internal-reflection technique for the examination of protein adsorption. J Biomed Mater Res **11:** 915–938

Wiegand UK, Don-Wauchope A, Matskevich I, Duncan RR, Greaves J, Shipston MJ, Apps DK, Chow RH (2002) Exocytosis studies in a chromaffin cell-free system: imaging of single-vesicle exocytosis in a chromaffin cell-free system using total internal reflection fluorescence microscopy. Ann N Y Acad Sci **971:** 257–261

Wightman RM, Haynes CL (2004) Synaptic vesicles really do kiss and run. Nat Neurosci **7:** 321–322

Xia S, Xu L, Bai L, Xu ZQ, Xu T (2004) Labeling and dynamic imaging of synaptic vesicle-like microvesicles in PC12 cells using TIRFM. Brain Res **997:** 159–164

Xu Y, Zhang F, Su Z, McNew JA, Shin YK (2005) Hemifusion in SNARE-mediated membrane fusion. Nat Struct Mol Biol **12:** 417–422

Yarar D, Waterman-Storer CM, Schmid SL (2005) A dynamic actin cytoskeleton functions at multiple stages of clathrin-mediated endocytosis. Mol Biol Cell **16:** 964–975

Yasuhara H, Sonobe S, Shibaoka H (1995) Effects of brefeldin A on the formation of the cell plate in tobacco BY-2 cells. Eur J Cell Biol **66:** 274–281

Zanner R, Gratzl M, Prinz C (2004) Expression of the endocytic proteins dynamin and amphiphysin in rat gastric enterochromaffin-like cells. J Cell Sci **117:** 2369–2376

Zefirov AL, Abdrakhmanov MM, Grigor'ev PN (2004) Kiss-and-run quantal secretion in frog nerve-muscle synapse. Bull Exp Biol Med **137:** 107–110

Zenisek D, Horst NK, Merrifield C, Sterling P, Matthews G (2004) Visualizing synaptic ribbons in the living cell. J Neurosci **24:** 9752–9759